






RESEARCH ARTICLE | OCTOBER 20 2022

Ionic liquid modulation of exchange bias in epitaxial LaMnO_3 thin films

Special Collection: [Magneto-ionic and electrostatic gating of magnetism: Phenomena and devices](#)

Xu Wen Zhao ; Sheung Mei Ng; Lok Wing Wong; Hon Fai Wong; Yu Kuai Liu; Wang Fai Cheng; Chee Leung Mak ; Jiong Zhao ; Chi Wah Leung  



Appl. Phys. Lett. 121, 162406 (2022)

<https://doi.org/10.1063/5.0106859>



CrossMark

starting at
EUR 6.360,-



Grows with your experiment.
The MFLI Lock-in Amplifier.

Field-upgradeable options

- 5 MHz frequency extension
- Multi-frequency analysis
- PID controller
- Impedance analyzer

 Zurich Instruments

[Find out more](#)

Ionic liquid modulation of exchange bias in epitaxial LaMnO_3 thin films

Cite as: Appl. Phys. Lett. **121**, 162406 (2022); doi: [10.1063/5.0106859](https://doi.org/10.1063/5.0106859)

Submitted: 30 June 2022 · Accepted: 29 September 2022 ·

Published Online: 20 October 2022



View Online



Export Citation



CrossMark

Xu Wen Zhao,¹ Sheung Mei Ng,¹ Lok Wing Wong,¹ Hon Fai Wong,¹ Yu Kuai Liu,² Wang Fai Cheng,¹ Chee Leung Mak,¹ Jiong Zhao,¹ and Chi Wah Leung^{1,a)}

AFFILIATIONS

¹Department of Applied Physics, the Hong Kong Polytechnic University, Hung Hom, Hong Kong, China

²College of Electronic Information and Mechatronics Engineering, Zhaoqing University, Zhaoqing 526061, Guangdong, China

Note: This paper is part of the APL Special Collection on Magneto-ionic and electrostatic gating of magnetism: phenomena and devices.

^{a)}Author to whom correspondence should be addressed: dennis.leung@polyu.edu.hk

ABSTRACT

The magnetic ground state of LaMnO_3 (LMO) thin film is still a controversial issue, even though various mechanisms, such as cation/anion non-stoichiometry, epitaxial strain, interfacial charge reconstruction, and orbital ordering, have been proposed. Here, exchange bias (EB) was introduced into a high-quality epitaxial LMO thin film via relatively low oxygen growth pressure. The EB in LMO was modulated by +2 V gating via ionic liquid method with increased EB field (H_{EB}), coercivity (H_C), blocking temperature (T_B), and reduced ferromagnetic (FM) magnetization. However, the −2 V gating has a much weaker tunability. By investigating the change of structure, surface morphology, and Mn oxidation state in LMO thin films, the modulation of magnetic properties is attributed to the creation/annihilation of oxygen vacancy in an LMO thin film. The suppressed FM phase in LMO can be ascribed to reduced Mn valence, structure disorders, and structure transition. However, the enriched antiferromagnetic phase results from the transition of the pseudocubic structure to the distorted orthorhombic structure. This work not only highlights the importance of functional defects in perovskite oxides but also sheds light on the potential of electric-field modulation of magnetism in spintronic devices.

Published under an exclusive license by AIP Publishing. <https://doi.org/10.1063/5.0106859>

As the parent compound of a magnetic perovskite manganite system, LaMnO_3 (LMO) has been widely studied due to the peculiar magnetic structure and transport properties.¹ LMO possesses an A-type antiferromagnetic (AF) structure with an ordering temperature ~ 140 K, as demonstrated by neutron scattering in bulk single crystals.^{2,3} However, robust ferromagnetism is detected in LMO thin films. With advanced thin film deposition techniques, the magnetic properties of high-quality LMO films have been investigated by controlling the strain state,^{4,5} La stoichiometry,^{6–8} oxygen stoichiometry,^{4,5,9–12} and polar discontinuity at the interfaces.^{13–15} Some suggested mechanisms of ferromagnetism in LMO thin films include (i) excess oxygen (in form of $\text{LaMnO}_{3+\delta}$) introduces Mn^{4+} ions and boosts the $\text{Mn}^{4+}\text{--O--Mn}^{3+}$ dominated double exchange interaction;⁹ (ii) La deficiency in the form of $(\text{La}^{3+}\text{Mn}^{2+})(\text{Mn}^{3+}\text{Mn}^{4+})\text{O}_3$ and similar to electron-doped ferromagnetic (FM) manganite;^{6–8} (iii) polar discontinuity leading to the interface charge reconstruction and electron doping, which boosts $\text{Mn}^{2+}\text{--O--Mn}^{3+}$ dominated double exchange interaction at the interface;^{13–17} and (iv) FM phase (P21/n) due to G-type $d_{3z^2-r^2}/d_{x^2-y^2}$ orbital ordering.^{18,19}

Although LMO thin films exhibit fascinating ferromagnetism, AF phase can still be traced through exchange bias (EB) effect.^{5,19–21} Regulation of EB in LMO thin films was usually demonstrated by deoxygenation via either post-annealing process or irradiation.^{5,9,21} It is of interest to explore potential voltage control of oxygen vacancies in LMO thin films, thus regulating their magnetism. For example, ionic liquid (IL) gating has been demonstrated as a powerful means to control the oxygen vacancy in transition metal oxides.^{22–24} However, explorations of ionic liquid modulation of EB in LMO thin films were rare, and the regulation mechanism was not very clear. The prospect of realization of IL regulation of EB in LMO thin films can not only offer a promising routes for low-power spintronic applications but can enrich our understanding of how oxygen vacancies mediate the complicated magnetism in LMO thin films.

Here, we deployed IL to create oxygen vacancies in LMO thin films with the goal of regulating the EB effect. High-quality epitaxial LMO thin films were prepared, and the EB effect in the films was confirmed by magnetic hysteresis (M – H) loop measurements of as-deposited samples. The EB can be enhanced by +2 V IL gating with

enhanced blocking temperature (T_B), increased EB field (H_{EB}), enlarged coercivity (H_C), and suppressed FM magnetization, whereas -2 V IL gating shows insignificant tunability.

Figure 1(a) shows the device structure for IL gating of LMO thin films. 2 V voltage was chosen since it lies within the electrochemical reaction region while keeping a relatively small leakage current (Fig. S1). According to previous reports,^{25,26} the modulation thickness via IL method based on electrochemical effects is at the order of 10 nm for oxides. Therefore, LMO (10 nm) thin films [Fig. S2(a)] were grown on NSTO (001) substrates. Atomic force microscopy (AFM) image of the as-grown LMO thin film [Fig. S2(b)] display atomically flat surfaces. After capping 2 -nm SiO_2 layer on LMO for sacrificial protection, 2θ scan profile over an extended range [Fig. S3(a) top panel] only shows (001) diffraction peaks, demonstrating the single phase. The narrow rocking curve around the (001) peak [$\sim 0.1^\circ$, Fig. S3(c)] suggests low mosaic spread.

The effect of IL gating on the crystal structure and morphology was first examined. For this purpose, an LMO thin film was first gated at -2 V for 1 h, and then a $+2$ V gate was applied on the same sample for another hour. 2θ scan profile [Fig. S3(a)] shows that neither -2 V nor $+2$ V IL gating created any observable impurity phase. The film thickness [Fig. S3(b)] and surface roughness (Fig. S4) were maintained through the gating steps as compared with the SiO_2 -capped pristine sample, suggesting moderate electrochemical process and no obvious surface degradation.²⁷ (001) diffraction peaks at different gating states [Fig. 1(b)] reveal that -2 V IL gating (middle panel) has negligible impact on the peak position ($2\theta = 22.64^\circ$) (top panel), while $+2$ V IL

gating (bottom panel) shifts the diffraction peak to a lower value ($2\theta = 22.44^\circ$) and hence an increased out-of-plane lattice constant.

Reciprocal space mapping (RSM) maps for asymmetric (103) lattice plane at different gating states were also recorded [Figs. 1(c)–1(e)]. It is observed that IL gating does not change the fully strained state of the LMO thin film, since all spot centers of LMO line up with that of NSTO in Q_x direction. The evolution of in-plane and out-of-plane lattice constants and the unit cell volume are depicted in Fig. 1(f). $+2$ V IL gating results in a tetragonal distortion of LMO unit cell along c -axis, while -2 V IL gating shows little impact. Qualitatively, the width of LMO spot distribution perpendicular to the [103] scattering vector is increased after IL gating. This means reduced crystallinity, which is partially reflected through the rocking curves around (001) diffraction peaks [Figs. S3(c)–S3(e)].

Figure 2(a) shows the IL gating process for magneto-transport measurements. Starting from the pristine state (State 1), voltage signals of -2 V and $+2$ V were applied alternatively to the film (one hour for each stage), leading to different states of the sample (States 2–5). M - H loops of the LMO thin film at different states are plotted in Fig. 2(b), and Table I summarizes important parameters extracted from the plots. In the pristine state (State 1), a square loop ($M_r/M_s = 0.92$, where M_r and M_s represent the remnant and saturated magnetization, respectively) is shown. The -2 V IL gating (State 2) has little impact on the magnetic properties, as testified by the virtually overlapping M - H loops in States 1 and 2. A subsequent $+2$ V IL gating process (State 3) results in a suppression of M_s and M_r alongside a huge increase in H_C , which is a clear sign of suppressed ferromagnetism.

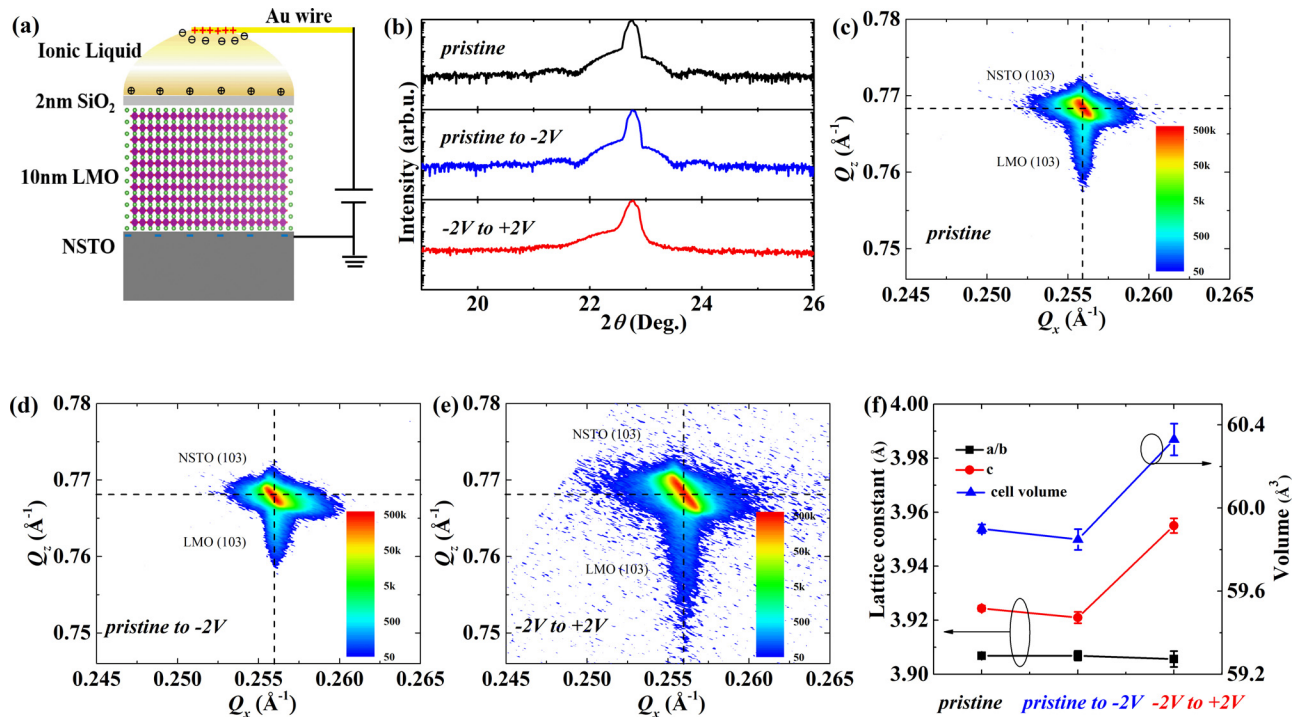


FIG. 1. (a) Device geometry for IL gating. (b) Out-of-plane 2θ scan profiles around NSTO (001) for an LMO sample at pristine state (top panel), followed by first a -2 V gating (middle panel) and then $+2$ V gating (bottom panel). (c)–(e) Asymmetric (103) RSM maps for the same LMO thin film at different states, after the sequence of IL gating processes. (f) Lattice parameters of the LMO thin film at different states.

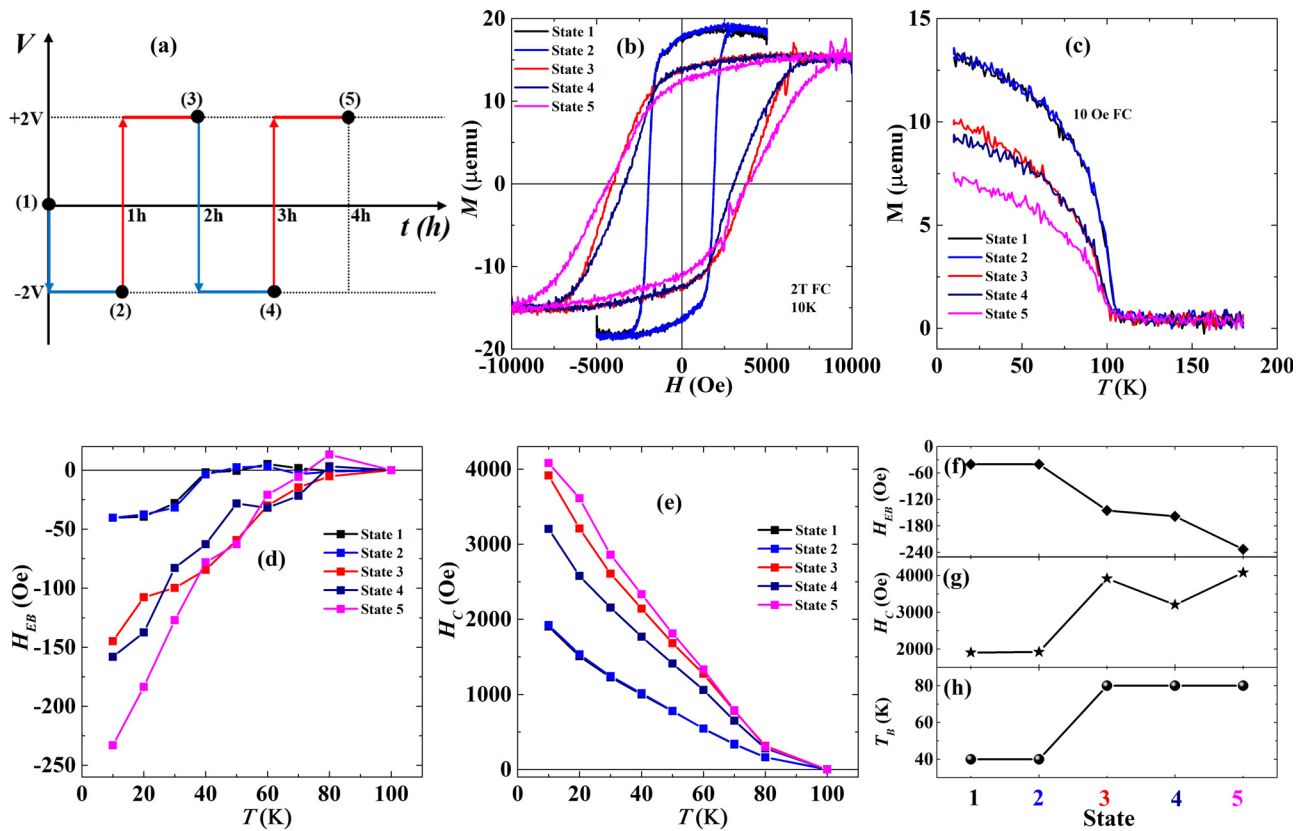


FIG. 2. (a) IL gating process for magneto-transport measurement. (b)–(e) M – H loops at 10 K, M – T curves with a 10-Oe applied field, temperature-dependent H_{EB} and H_C of LMO film at different states, respectively. (f)–(h) Evolution of the H_{EB} at 10 K, H_C at 10 K, and T_B at different states.

To verify whether the reduced ferromagnetism can be restored, a second -2 V IL gating process was applied (State 4). While H_C is slightly reduced to 3200 Oe, both M_s and M_r keep unchanged compared with State 3. A second $+2$ V IL gating (State 5) results in unchanged M_s , but the M_r (H_C) is slightly reduced (increased), which suggests the magnetism is further altered. The effect is also reflected through temperature-dependent magnetization (M – T) curves measured at various states [Fig. 2(c)]. The magnetization below Curie temperature (T_C) is suppressed by $+2$ V IL gating while -2 V IL gating shows a weak effect. Furthermore, M – T curves at different states all diminish at ~ 110 K, suggesting that IL gating does not affect the T_C in the LMO thin film.

We define EB field as $H_{EB} = (H_2 + H_1)/2$, where H_2 is the negative coercive field while H_1 represents the positive one. The coercivity is defined as $H_C = (H_1 - H_2)/2$. Figures 2(d) and 2(e) depict the

TABLE I. M_r , M_s , and M_r/M_s ratio of the LMO thin film for different states at 10 K.

	State 1	State 2	State 3	State 4	State 5
M_r (μemu)	17.5	17.5	13.5	13.5	12.4
M_s (μemu)	19.1	19.1	15.8	15.8	15.8
M_r/M_s	0.92	0.92	0.85	0.85	0.78
H_C (Oe)	1900	1920	3920	3200	4080

temperature-dependent H_{EB} and H_C . For State 1, the LMO thin film shows a small H_{EB} , suggesting the coexistence of AF and FM phase as reported before.^{19–21} H_{EB} disappears at around 40 K (the blocking temperature, T_B), which is far less than the AF ordering temperature of bulk LMO but is close to previously reported T_B in oxygen deficient LMO films.^{5,20} After the first -2 V IL gating (State 2), both temperature-dependent H_{EB} and H_C curves overlap with those of state 1, indicating no change of magnetic properties. However, after the first $+2$ V IL gating (State 3), the H_{EB} is significantly increased along with an enhanced T_B (from 40 to 80 K). The temperature-dependent H_C also shows an increase. For the second -2 V IL gating (State 4), only temperature-dependent H_C is slightly reduced from State 3. The temperature-dependent H_{EB} does not exhibit an obvious reduction compared with State 3. In contrast, at low temperatures, the H_{EB} continues to increase even after -2 V IL gating. For the second $+2$ V IL gating (State 5), temperature-dependent H_{EB} and H_C are increased at low temperatures from State 4. The evolution of H_{EB} and H_C at 10 K are plotted in Figs. 2(f) and 2(g), respectively. The evolution of T_B is depicted in Fig. 2(h). A sharp increase in T_B only occurs after the first $+2$ V IL gating (State 3); and further IL gating shows no effect.

According to the classical model of the EB,²⁸ H_{EB} is inversely related to M_s in FM. Assuming that IL gating does not change the AF phase, then the effect of IL gating on H_{EB} should be closely linked with M_s . From State 2 to State 3, M_s is suppressed by $+2$ V IL gating and

H_{EB} is therefore enhanced. But from State 4 to State 5, M_s is not changed by +2 V IL gating (Table I) while the H_{EB} still show an increase, suggesting that the suppressed FM phase and enriched AF phase should act cooperatively for the enhanced EB effect.

Normally there are two mechanisms for pure IL gating devices: electrostatic doping and electrochemical reactions. Since the gating voltage used in the work is in the electrochemical regime (Fig. S1), and as all our measurements were conducted after removing IL, electrostatic doping can be ruled out. Redox-based electrochemical reaction has been widely reported in many transition metal oxide systems.^{23,29,30} The removal/injection of oxygen ions not only results in structural transformation but also leads to the change of oxidation state for transition metal ions.^{29,31} To this end, electron energy loss spectroscopy (EELS) and transmission electron microscopy (TEM) studies were carried out on LMO thin films under three conditions. The first sample is the as-prepared LMO thin film and can be regarded as the pristine state. The second sample was gated from pristine state by -2 V for one hour in vacuum at 300 K and is taken as -2 V IL gated state. The last sample was gated from pristine state by +2 V for one hour in vacuum at 300 K and is taken as +2 V IL gated state.

Since oxygen vacancies are strongly correlated with the oxidation state of Mn ions, EELS along LMO thickness direction were performed to investigate the influence of IL gating on Mn valence states. The realigned Mn $L_{3,2}$ edges based on the pre-peak position of O K edge

(around 530 eV for O_{2p} - Mn_{3d} hybridization, Fig. S5) are plotted in Figs. 3(a)–3(c). For the pristine state [Fig. 3(a)], the sample exhibits a red shift at the interface (white line at 1 nm) and surface (white line at 9 nm) compared with these white lines located at the middle. According to previous reports,^{12,15,16,32,33} the low oxidation state of Mn ions at interface can originate from the electronic reconstruction due to polar discontinuity, while the low Mn oxidation state at the surface arises from oxygen vacancies due to surface symmetry breaking. For -2 V IL gated state [Fig. 3(b)], all white lines show a shift toward higher energy. For +2 V IL gated state [Fig. 3(c)], all white lines shift toward lower energy compared with the pristine state, and the low oxidation states of Mn ions at the interface and surface are maintained.

To quantitatively understand the effect of IL gating on the oxidation state of Mn ions, a fitting method (details in Fig. S6) was deployed to obtain the L_3 peak position [Fig. 3(d)]. From Fig. 3(d), the L_3 peak positions for +2 V IL gated sample shift to around 640.5 eV, about 0.7 eV lower than that of pristine state. For the -2 V IL gated sample, the L_3 peak positions do not show obvious changes as compared with those of pristine state. Multivalence states (+2, +3, and +4) of Mn ions are possible in LMO films due to oxygen non-stoichiometry and interfacial charge reconstruction.^{4,15,16} Most studies have ascribed ferromagnetism in LMO thin films to this multivalence state of Mn ions. Therefore, we extracted the L_3/L_2 ratio [Fig. 3(e)] to investigate how IL gating affects the oxidation state of Mn ions. Within the bulk of the

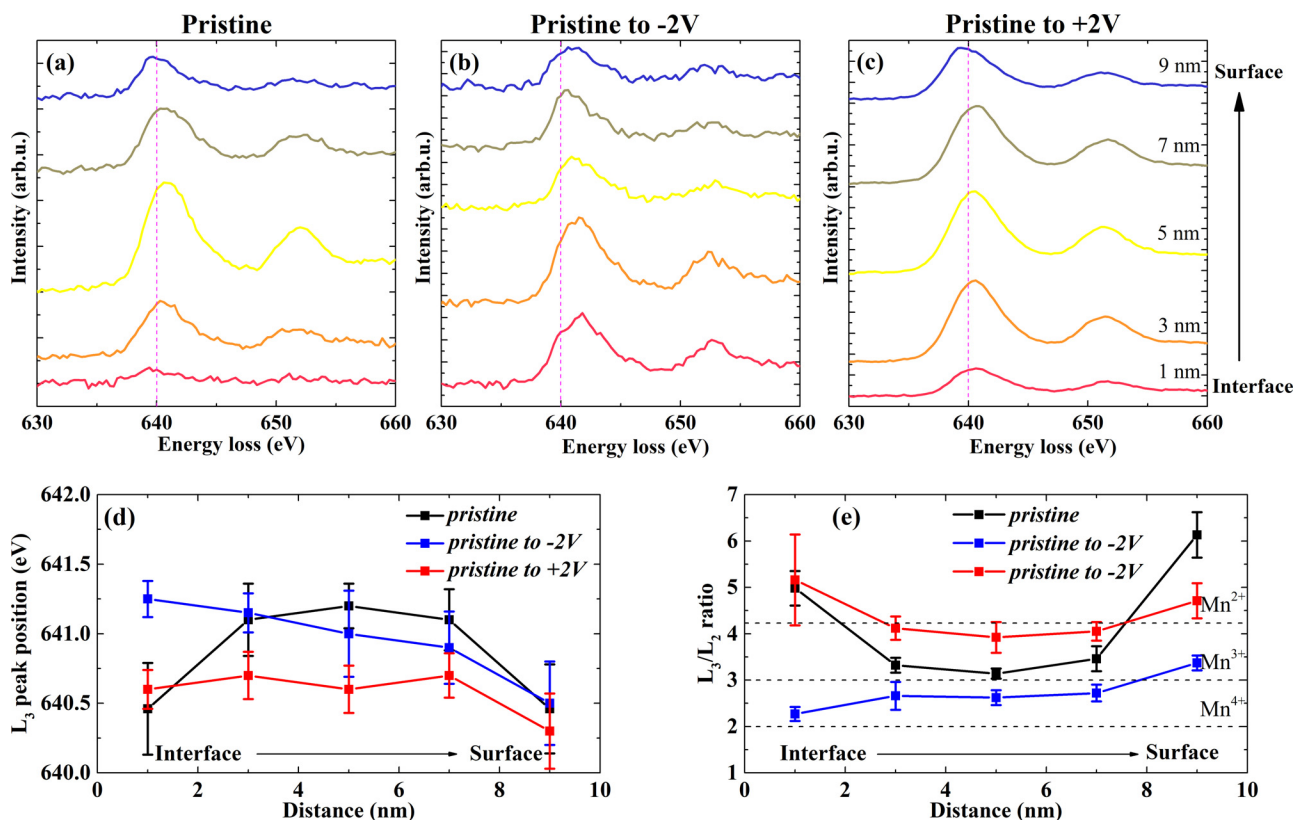


FIG. 3. The Mn L edge white lines from the interface to the top surface for pristine (a), -2 V gated (b), and +2 V gated states (c). (d) and (e) The depth-dependent L_3 peak position and the extracted L_3/L_2 ratio for pristine state (black), -2 V IL gated state (blue), and +2 V IL gated state (red).

pristine sample, the value of L_3/L_2 is about 3.1 rather than 3, which could be ascribed to the relatively low oxygen growth condition. The characteristic of interfacial electronic reconstruction is confirmed, which cannot be removed even with +2 V IL gating. According to previous report,¹⁵ different L_3/L_2 ratios in Fig. 3(e) can be representative for different valence states of Mn ions in LMO (4.2 for Mn^{2+} , 3 for Mn^{3+} , and 2 for Mn^{4+}). Compared with the pristine state, the L_3/L_2 ratio for -2 V IL gated state show a distribution from 2 to 4.2, suggesting the coexistence of multivalence states (+2, +3, and +4) of Mn ions. While for the pristine and +2 V gated state, +3 and +2 are dominant valence states, respectively.

The magnetic properties of perovskite manganites are closely linked to the exchange interactions between Mn spins via oxygen ions. The variation of Mn valence is considered as a key factor for different magnetic properties. For +2 V IL gated state, the reduced valence from +3 to +2 suppresses the double exchange-dominated ferromagnetism, which is consistent with magneto-transport results (Fig. 2). For -2 V IL gated state, the coexistence of multivalence suggests enhanced ferromagnetism, which is, however, contrary to the magneto-transport results (state 2 in Fig. 2). In addition, for +2 V IL gated state, the superexchange-dominated AF phase should be suppressed due to reduced $\text{Mn}^{3+}\text{-O-Mn}^{3+}$ chains, which is also contrary to the cooperation of the suppressed FM phase and enriched AF phase discussed above. These analyses indicate that apart from variation of Mn valence state, there are other contributions to the variation of magnetic properties during IL gating process.

Representative Fourier-filtered images and the corresponding cross-sectional TEM images are shown in Fig. 4. Dislocations (marked as \perp) can be found in IL gated LMO thin films [Figs. 4(b) and 4(c)]

compared with pristine state [Fig. 4(a)]. Although the -2 V IL gating has little effect on lattice constant [Fig. 1(f)], structural dislocations are still induced and is consistent with the RSM results [Fig. 1(d)]. These observed structural disorders can explain why ferromagnetism is not enhanced for -2 V IL gated state. From the cross-sectional TEM images, one can see that the LMO lattices keep a coherent relationship with the NSTO, which again confirms the RSM results [Figs. 1(c)–1(e)]. Meanwhile, the +2 V IL gated LMO film shows extra $\frac{1}{2}(011)_{pc}$ (pc represents pseudocubic) spots from the fast Fourier transform (FFT) spot patterns [inset of Fig. 4(f)]. This indicates a different structural phase induced by +2 V IL gating. These extra $\frac{1}{2}(011)_{pc}$ reflections were only reported in LMO related superlattices,^{34–36} which is ascribed to the transformation from the pseudocubic structure to the orthorhombic structure due to in-phase octahedral rotation. In our case, +2 V IL gating leads to the expansion of LMO unit cell along the out-of-plane direction due to larger Mn^{2+} ionic radius.⁵ This unit cell expansion is accommodated by oxygen octahedral distortion, which is confirmed by XRD (Fig. S7).

The inverse fast Fourier transform (IFFT) images of normal pseudocubic spots [green circled spots in Fig. S8(b)] and the $\frac{1}{2}(011)_{pc}$ spots [red circled spots in Fig. S8(b)] from a large area [Fig. S8(a)] are extracted. By mixing the two IFFT images together [Fig. S8(c)], the oxygen octahedral distortion is observed throughout LMO films with different degrees of distortion. Line scan profiles along vertical and horizontal direction of the two IFFT images are obtained to study the corresponding basis arrangement. For horizontal direction [Fig. S8(d)], it is observed that the distance between basis for extra $\frac{1}{2}(011)_{pc}$ spots is doubled. Moreover, there is a small gap between peak

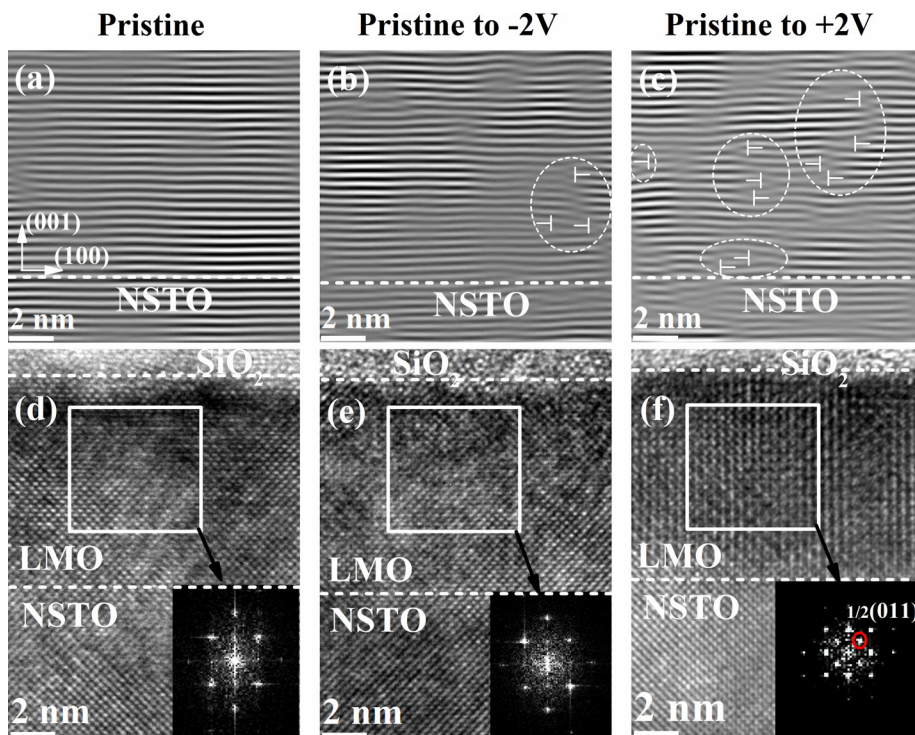


FIG. 4. Fourier-filtered images for the pristine state (a), -2 V IL gated state (b), and +2 V IL gated state (c). The corresponding cross section TEM images are shown in (d)–(f), respectively. Inset: the FFT spot pattern corresponding to the enclosed regions.

positions of two series of basis. A similar phenomenon is also observed along the vertical direction [Fig. S8(e)].

Based on the above analysis, the distorted orthorhombic structure with $2a_{pc} \times 2a_{pc}$ can be plotted in Fig. S8(f), which shows similar octahedral distortion with that in LMO based superlattices.³⁶ Compared with the pseudocubic structure, the octahedral distortion leads to increase Mn–O bond length and reduction of Mn–O–Mn bond angle for both in-plane and out-of-plane directions. According to previous report,³⁴ the increased Mn–O bond length and reduced Mn–O–Mn bond angle can significantly quench the ferromagnetism in LMO layer. The increased bond length and reduced bond angle in +2 V IL gated LMO film means more overlapped orbital between Mn-3d and O-2p, which could be the reason for enriched AF phase in +2 V IL gated LMO films. Further studies about the structure and its magnetic properties are needed.

In summary, high-quality epitaxial LMO thin films exhibiting the EB effect are prepared. By using IL gating, the crystal structure, structure disorders, Mn oxidation state, and magnetic properties of LMO thin films are regulated. +2 V IL gating suppresses the EB effect by suppressing the FM phase and enriching the AF phase. The enhanced AF phase is possibly associated with the structure transition from the pseudocubic phase to the distorted orthorhombic phase because of increased oxygen vacancies. This work offers the possibility to control the antiferromagnetic spintronic devices by defect engineering.

See the [supplementary material](#) for more details about experimental method, additional characterization, and additional analysis of the extra $\frac{1}{2}(011)$ reflections.

This work was supported by the Hong Kong Research Grants Council (No. PolyU 153027/17P), the Hong Kong Polytechnic University (1-ZVWC, G-UAG), ZVGH, ZVRP, and ZVQH), the Research Fund of Zhaoqing University (No. 2021011832), and the Guangdong Special Support Project (No. 2019BT02X030).

AUTHOR DECLARATIONS

Conflict of Interest

The authors have no conflicts to disclose.

Author Contributions

Xu Wen Zhao: Conceptualization (equal); Data curation (lead); Formal analysis (lead); Investigation (lead); Methodology (lead); Writing – original draft (lead); Writing – review & editing (equal). **Sheung Mei Ng:** Data curation (equal); Formal analysis (equal); Methodology (equal). **Lok Wing Wong:** Data curation (equal); Formal analysis (equal). **H. F. Wong:** Data curation (equal); Formal analysis (equal); Methodology (supporting). **Y. K. Liu:** Formal analysis (supporting); Methodology (supporting). **Wang Fai Cheng:** Methodology (supporting). **Chee Leung Mak:** Data curation (equal); Resources (equal). **Jiong Zhao:** Data curation (equal); Resources (equal). **Chi Wah Leung:** Conceptualization (lead); Formal analysis (lead); Funding acquisition (lead); Investigation (lead); Methodology (lead); Project administration (lead); Resources (lead); Supervision (lead); Writing – review & editing (lead).

DATA AVAILABILITY

The data that support the findings of this study are available from the corresponding author upon reasonable request.

REFERENCES

- Y. Tokura and N. Nagaosa, *Science* **288**, 462 (2000).
- E. O. Wollan and W. C. Koehler, *Phys. Rev.* **100**, 545 (1955).
- F. Moussa, M. Hennion, J. Rodriguez-Carvajal, and H. Moudden, *Phys. Rev. B* **54**, 15149 (1996).
- W. Niu, W. Liu, M. Gu, Y. Chen, X. Zhang, M. Zhang, Y. Chen, J. Wang, J. Du, F. Song, X. Pan, N. Pryds, X. Wang, P. Wang, Y. Xu, Y. Chen, and R. Zhang, *Adv. Electron. Mater.* **4**, 1800055 (2018).
- Y. K. Liu, H. F. Wong, K. K. Lam, C. L. Mak, and C. W. Leung, *J. Magn. Magn. Mater.* **481**, 85 (2019).
- P. Orgiani, C. Aruta, R. Ciancio, A. Galdi, and L. Maritato, *Appl. Phys. Lett.* **95**, 013510 (2009).
- P. Orgiani, A. Galdi, C. Aruta, V. Cataudella, G. De Filippis, C. A. Perroni, V. Marigliano Ramaglia, R. Ciancio, N. B. Brookes, M. Moretti Sala, G. Ghiringhelli, and L. Maritato, *Phys. Rev. B* **82**, 205122 (2010).
- I. Marozau, P. T. Das, M. Döbeli, J. G. Storey, M. A. Uribe-Laverde, S. Das, C. Wang, M. Rösle, and C. Bernhard, *Phys. Rev. B* **89**, 174422 (2014).
- W. S. Choi, Z. Marton, S. Y. Jang, S. J. Moon, B. C. Jeon, J. H. Shin, S. S. A. Seo, T. W. Noh, K. Myung-Whun, H. N. Lee, and Y. S. Lee, *J. Phys. D* **42**, 165401 (2009).
- H. S. Kim and H. M. Christen, *J. Phys.: Condens. Matter* **22**, 146007 (2010).
- R. Zhao, K. Jin, Z. Xu, H. Guo, L. Wang, C. Ge, H. Lu, and G. Yang, *Appl. Phys. Lett.* **102**, 122402 (2013).
- J. Peng, C. Song, F. Li, Y. D. Gu, G. Y. Wang, and F. Pan, *Phys. Rev. B* **94**, 214404 (2016).
- X. R. Wang, C. J. Li, W. M. Lü, T. R. Paudel, D. P. Leusink, M. Hoek, N. Poccia, A. Vailionis, T. Venkatesan, J. M. D. Coey, E. Y. Tsymlal, Ariando, and H. Hilgkamp, *Science* **349**, 716 (2015).
- L. Wu, C. Li, J. Ma, C. Nan, and X. R. Wang, *Sci. Bull.* **63**, 949 (2018).
- M. Li, C. Tang, T. R. Paudel, D. Song, W. Lu, K. Han, Z. Huang, S. Zeng, X. R. Wang, P. Yang, Ariando, J. Chen, T. Venkatesan, E. Y. Tsymlal, C. Li, and S. J. Pennycook, *Adv. Mater.* **31**, e1901386 (2019).
- Z. Chen, Z. Chen, Z. Q. Liu, M. E. Holtz, C. J. Li, X. R. Wang, W. M. Lu, M. Motapothula, L. S. Fan, J. A. Turcaud, L. R. Dedon, C. Frederick, R. J. Xu, R. Gao, A. T. N'Diaye, E. Arenholz, J. A. Mundy, T. Venkatesan, D. A. Muller, L. W. Wang, J. Liu, and L. W. Martin, *Phys. Rev. Lett.* **119**, 156801 (2017).
- Y. Anahory, L. Embon, C. J. Li, S. Banerjee, A. Meltzer, H. R. Naren, A. Yakovenko, J. Cuppens, Y. Myasoedov, M. L. Rappaport, M. E. Huber, K. Michaeli, T. Venkatesan, Ariando, and E. Zeldov, *Nat. Commun.* **7**, 12566 (2016).
- Y. S. Hou, H. J. Xiang, and X. G. Gong, *Phys. Rev. B* **89**, 064415 (2014).
- M. Yang, K. Jin, H. Yao, Q. Zhang, Y. Ji, L. Gu, W. Ren, J. Zhao, J. Wang, E. J. Guo, C. Ge, C. Wang, X. Xu, Q. Wu, and G. Yang, *Adv. Sci.* **8**, 2100177 (2021).
- J. Peng, C. Song, B. Cui, F. Li, H. J. Mao, Y. Y. Wang, G. Y. Wang, and F. Pan, *Phys. Rev. B* **89**, 165129 (2014).
- M. Xue, S. Ding, Y. Lai, X. Li, L. Zha, Y. Peng, Z. Liang, W. Yang, Y. Men, X. Kong, L. Han, X. Chen, and J. Yang, *Adv. Mater. Interfaces* **7**, 1901296 (2020).
- J. Jeong, N. Aetukuri, T. Graf, T. D. Schladt, M. G. Samant, and S. S. P. Parkin, *Science* **339**, 1402 (2013).
- B. Cui, C. Song, G. Wang, Y. Yan, J. Peng, J. Miao, H. Mao, F. Li, C. Chen, F. Zeng, and F. Pan, *Adv. Funct. Mater.* **24**, 7233 (2014).
- C. Leighton, *Nat. Mater.* **18**, 13 (2019).
- C. Song, B. Cui, F. Li, X. Zhou, and F. Pan, *Prog. Mater. Sci.* **87**, 33 (2017).
- Y. Gu, K. Xu, C. Song, X. Zhong, H. Zhang, H. Mao, M. S. Saleem, J. Sun, W. Liu, Z. Zhang, F. Pan, and J. Zhu, *ACS Appl. Mater. Interfaces* **11**, 19584 (2019).
- S. Zhao, Z. Zhou, B. Peng, M. Zhu, M. Feng, Q. Yang, Y. Yan, W. Ren, Z. G. Ye, Y. Liu, and M. Liu, *Adv. Mater.* **29**, 1606478 (2017).
- W. H. Meiklejohn and C. P. Bean, *Phys. Rev.* **105**, 904 (1957).
- B. Cui, P. Werner, T. Ma, X. Zhong, Z. Wang, J. M. Taylor, Y. Zhuang, and S. S. P. Parkin, *Nat. Commun.* **9**, 3055 (2018).

- ³⁰L. Zhu, L. Gao, L. Wang, Z. Xu, J. Wang, X. Li, L. Liao, T. Huang, H. Huang, A. Ji, N. Lu, Z. Cao, Q. Li, J.-R. Sun, P. Yu, and X. Bai, *Chem. Mater.* **33**, 3113 (2021).
- ³¹L. Yao, S. Inkinen, and S. van Dijken, *Nat. Commun.* **8**, 14544 (2017).
- ³²A. Sadoc, B. Mercey, C. Simon, D. Grebille, W. Prellier, and M. B. Lepetit, *Phys. Rev. Lett.* **104**, 046804 (2010).
- ³³M. J. Calderon, L. Brey, and F. Guinea, *Phys. Rev. B* **60**, 6698 (1999).
- ³⁴X. Zhai, L. Cheng, Y. Liu, C. M. Schlepütz, S. Dong, H. Li, X. Zhang, S. Chu, L. Zheng, J. Zhang, A. Zhao, H. Hong, A. Bhattacharya, J. N. Eckstein, and C. Zeng, *Nat. Commun.* **5**, 4283 (2014).
- ³⁵J. Verbeeck, O. I. Lebedev, G. Van Tendeloo, and B. Mercey, *Phys. Rev. B* **66**, 184426 (2002).
- ³⁶X. Guan, X. Shen, J. Zhang, W. Wang, J. Zhang, H. Wang, W. Wang, Y. Yao, J. Li, C. Gu, J. Sun, and R. Yu, *Phys. Rev. B* **100**, 014427 (2019).